

Common- and Differential-Mode HF Current Components in AC Motors Supplied by Voltage Source Inverters

Gabriele Grandi, *Member, IEEE*, Domenico Casadei, *Associate Member, IEEE*, and Ugo Reggiani, *Member, IEEE*

Abstract—In this paper, an inverter-fed ac motor drive is analyzed in order to investigate the conducted electromagnetic interferences at both the input and output sides of the inverter. HF lumped equivalent circuits for the inverter and the motor stator windings are proposed. The overall circuit model allows time- and frequency-domain analysis to be performed with standard circuit simulators. The proposed model can also predict common- and differential-mode HF current components. The equivalent circuit is verified by experimental tests carried out on a prototype of ac motor drive.

Index Terms—Circuit model, common-mode, differential-mode, electromagnetic interference, frequency-domain analysis, HF, inverter, motor stator windings, time-domain analysis.

I. INTRODUCTION

NOWADAYS, ac motor drives are widely used in electromechanical energy conversion systems. Modern power electronic inverters are based on PWM techniques with switches characterized by very small switching times. As a consequence, the motor windings are subjected to a very large amount of HF voltage components [1], [2]. Owing to parasitic winding capacitances [3] (i.e., turn-to-turn and turn-to-ground capacitances), these HF voltage components cause HF leakage currents [4] and conducted electromagnetic interferences (EMI) in the power mains and ground system [5]–[7]. The resulting HF currents are classified in common- and differential-mode (CM and DM) components according to their circulation paths [8]–[10]. The frequency range of interest for conducted EMI in power electronics is usually from tens of kilohertz up to tens of megahertz [11]. Owing to the high switching speed of MOSFETs and IGBTs, the nonideal behavior of the power converter plays an important role in the HF current component prediction. Thus, in order to model the HF behavior of the converter, it is necessary to take account of parasitic parameters in semiconductor devices and passive elements of the power circuit [12].

In the low and medium power range, the low voltage induction motor is the most frequently used type of motor. In this case, the stator windings are realized by a series connection of mush wound coils. Because of the random distribution of the turns in each coil, an analytical evaluation of the coil model parameters cannot be based on single-turn models such as in form wound

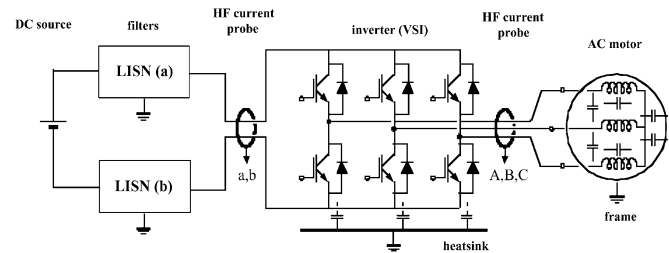


Fig. 1. Inverter-fed induction motor drive with LISNs.

coils [13], [14]. Hence, the lumped equivalent circuit of a mush wound coil can be defined in terms of equivalent impedance by means of a suitable three-terminal network. Both the real and imaginary parts of the impedance should be considered to properly model the coil behavior [15]. The model of a multi-coil stator winding can be derived from the single-coil model [16]. A three-phase induction motor can be regarded as a “black box” with one terminal for each motor phase and a terminal for the motor frame (ground). Thus, the equivalence between the model and the stator windings is formulated in terms of phase-to-phase and phase-to-ground impedances.

The system analyzed in this paper is shown in Fig. 1. Two line impedance stabilization networks (LISNs, $50 \Omega/50 \mu\text{H}$) are employed to decouple the dc source from the inverter. The proposed circuit model includes both the inverter and the induction motor. The HF current interferences at the input and output sides of the inverter are numerically evaluated by PSpice. In particular, common- and differential-mode current components are considered in order to emphasize the HF coupling between the dc link and the motor terminals. A time domain analysis is carried out together with a frequency-domain analysis to determine the HF current harmonic spectrum. The calculated results are compared with the experimental tests obtained with a drive system prototype.

II. HF CIRCUIT MODELS

In the system analyzed in this paper the length of the two cables connecting the LISNs to the inverter and the length of the three cables feeding the motor are about 1 m. These power connections are simply modeled by series RL circuits. More detailed circuit models for the inverter and the motor stator windings are developed in the following sections [17]–[20].

A. Inverter Model

In [12] an accurate circuit model for a switching cell, which is the basic structure of most power converters, has been presented

Manuscript received November 8, 2002; revised April 21, 2003. Recommended by Associate Editor M. G. Simoes.

The authors are with the Department of Electrical Engineering, University of Bologna, Bologna 2-40136, Italy.

Digital Object Identifier 10.1109/TPEL.2003.820564

TABLE I
THREE-PHASE INVERTER RATINGS

	Type	Max. Voltage	Max. Current
IGBT (+diode):	3x SKM200GB122D	1200 V	150 A
Driver:	3x SKHI21		
Capacitors:	Electrolytic: 1.5mF, Ceramic: 0.33 μ F		
Heatsink:	P16/300F - Forced air cooling		

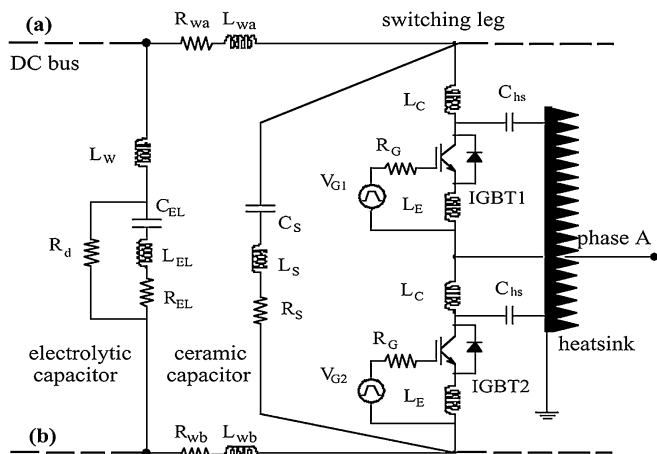


Fig. 2. HF circuit model for an inverter leg with parasitics.

TABLE II
THREE-PHASE INDUCTION MOTOR DATA

Power	Voltage, Frequency	Speed	Cooling
4 kW	220/380 V, 50 Hz	2800 rpm	coaxial fan

and validated by experimental tests. In this paper the equivalent circuit of the three-phase voltage source inverter (VSI) is obtained by an extension of the switching cell model. The ratings and the main characteristics of the inverter are given in Table I. Fig. 2 shows the HF equivalent circuit for one leg of the three-phase inverter. The corresponding parameter values are summarized in Table III. Each leg of the three-phase inverter consists of two power IGBTs with parallel freewheeling diodes. The models adopted for IGBTs and diodes are the PSpice general models [21]. These models were fitted with the parameter values given in the data sheets by using the “Parts” utility of PSpice [21]. The effects of the IGBT and diode internal capacitances are included in the PSpice model, whereas the values of the collector and emitter internal inductances, L_C and L_E , have been introduced in the inverter model on the basis of additional experimental data [22].

The main parasitic components of the proposed HF circuit model represented in Fig. 2 are as follows.

- *Stray inductances of the connecting wires.* These parameters affect the total inductance of the circuit loops and are strongly dependent on the converter layout. It is possible to evaluate these inductances (L_{wa} and L_{wb}) by the analytical formula for two parallel cylindrical conductors or for a circular or rectangular single-turn loop.

- *Parasitic inductances of the capacitors.* It is not usually possible to evaluate these inductances analytically, but they can be measured by impedance meters. Typical values are $L_S = 5\text{--}20$ nH for ceramic capacitors and $L_{EL} = 30\text{--}100$ nH for large electrolytic capacitors [23].

A parallel connection of both capacitor types is usually employed to obtain a large equivalent capacitance with a low equivalent parasitic inductance.

- *Parasitic capacitances between the power switches and the ground.* The ground potential may be introduced (for safety reasons) by the heatsink of the power switches and the metallic chassis. The values of these capacitances can be evaluated by means of the parallel-plate capacitor formula. They depend on the size and geometry of power switches. In particular, for MOSFET or IGBT power modules the resulting collector-to-heatsink stray capacitance, C_{hs} , is in the order of hundreds of pF (measured).

B. Stator Winding Model

The stator winding model only is considered in this analysis because the HF magnetic fields practically do not penetrate the stator and rotor core laminations [15]. For this reason the magnetic couplings to be taken into account are those among the overhangs only. In the case of squirrel-cage induction motors, these magnetic couplings are significant only for the stator overhangs.

As far as the capacitive couplings are concerned, only the stator windings and the frame should be considered for modeling squirrel-cage induction motors. In particular, since the mush stator windings are usually placed inside semi-closed slots, almost completely surrounded by iron laminations, the main capacitive coupling of the stator is towards the iron frame. Furthermore, the capacitive coupling between the stator overhangs and the frame should be considered.

On the basis of these considerations, a three-phase motor can be regarded as a “black box” with one terminal for each stator phase and a terminal for the motor frame (ground). Thus, the equivalence between the model and the stator windings is formulated in terms of phase-to-phase and phase-to-ground complex impedances. Some impedance measurements on different stator windings have shown that the same topology of the single-coil equivalent circuit proposed in [15], consisting of the series connection of two resonators, can be adopted also for each phase of a three-phase motor, as represented in Fig. 3(a). In this paper the mutual inductive couplings among the stator phases are taken into account by introducing the mutual inductances M_1 and M_2 . The direct phase-to-phase capacitive couplings are neglected being the corresponding capacitances much lower than the phase-to-ground capacitances C_g . The resulting model valid for three-phase stator windings is shown in Fig. 3(b).

In order to make the three-phase winding model fit with the experimental data, an identification problem must be solved. The model fitting can be performed either by a trial-and-error method or numerical techniques. An initial estimate of the reactive parameters of the three-phase winding model can be obtained as follows.

1) *Self- and Mutual Phase Inductances:* The overall phase self-inductance $L_p = L_1 + L_2$ can be evaluated by impedance measurements at the phase terminals for frequencies lower than the first self-resonant frequency. This parameter is frequency-

TABLE III
NOMENCLATURE AND PARAMETER VALUES OF THE PROPOSED HF MODELS

INVERTER		
R_{was}, R_{wb}	3.9 m Ω	<i>dc-bus bars: stray resistances</i>
L_{was}, L_{wb}	0.36 μ H	<i>stray inductances</i>
C_{EL}	1500 μ F	<i>electrolytic capacitor: dc capacitance</i>
L_w	10 nH	<i>external wire inductance</i>
L_{EL}, R_{EL}	30 nH, 40 m Ω	<i>internal series inductance and resistance</i>
R_d	100 k Ω	<i>discharging resistance</i>
C_S	0.33 μ F	<i>ceramic capacitor: dc capacitance</i>
L_S, R_S	30 nH, 30 m Ω	<i>internal series inductance and resistance</i>
L_C, L_E	40 nH, 40 nH	<i>IGBTs: collector and emitter stray inductances</i>
R_G	64 Ω	<i>gate resistor</i>
V_{G1}, V_{G2}	0-15 V	<i>gate control voltages</i>
C_{hs}	280 pF	<i>IGBT to heatsink stray capacitance</i>
MOTOR		
C_g, R_g	300 pF, 12 Ω	<i>phase-to-ground stray capacitance and series resistance</i>
M_1, M_2	1.1 mH, 0.08 mH	<i>phase-to-phase mutual inductances of the two resonators</i>
R_{p1}, R_{p2}	4.8 k Ω , 2 k Ω	<i>parallel resistances of the two resonators</i>
C_1, C_2	560 pF, 380 pF	<i>stray capacitances of the two resonators</i>
R_{C1}, R_{C2}	10 Ω , 15 Ω	<i>series resistances (capacive branch)</i>
L_1, L_2	3.26 mH, 1.15 mH	<i>main inductances of the two resonators</i>
R_{L1}, R_{L2}	100 Ω , 80 Ω	<i>series resistances (inductive branch)</i>

dependent but an average value can be extrapolated and fixed in the considered frequency range.

Although there are impedance bridges that can measure the mutual inductance, a common method to determine M is based on measuring the equivalent inductance with different coil connections. This procedure leads to $M = (L' - L'')/4$, where L' and L'' represent the measured inductances when the two coils are connected in series with positive and negative mutual coupling, respectively.

2) *Phase-to-Ground Capacitances*: The capacitive coupling between each motor phase and the ground is represented by two lumped capacitances C_g at the beginning and the end of each phase [Fig. 3(b)]. The value of C_g can be evaluated by connecting the six terminals of the motor phases at the same node, and dividing by six the resulting capacitance C_{tg} measured between the node and the ground: $C_g = C_{tg}/6$. The value of C_{tg} practically corresponds to the phase-to-ground capacitance measured at low frequency (e.g., below the first self-resonance) from a motor terminal to ground. In fact, for either delta or star connections, the phase inductive reactance is negligible compared to the capacitive parallel reactance.

3) *Inner Phase Capacitances*: For high excitation frequencies (e.g., above the self-resonances), the input-to-output inner phase capacitance C_p is represented by the series of the capacitances C_1 and C_2 of the two resonators, as shown in Fig. 3(a). The evaluation of this capacitance can be carried out by measuring the capacitance C_{tp} between the terminals of two phases at a high frequency. Assuming star-connected motor phases yields

$$C_{tp} = \frac{1}{2}(C_g + C_p) \Rightarrow C_p = 2C_{tp} - C_g.$$

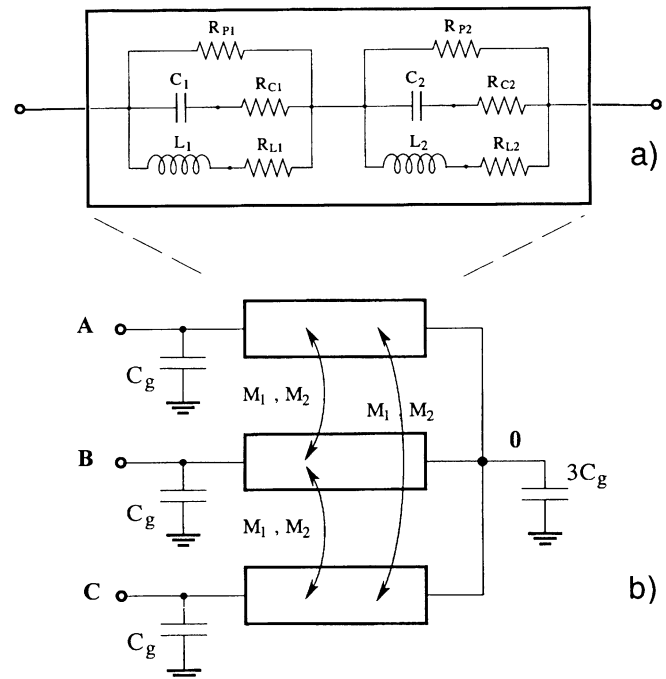


Fig. 3. Circuit model for a three-phase winding.

Both L_p and C_p must be split into L_1, L_2 , and C_1, C_2 , respectively, according to the equivalent circuit of Fig. 3(a). As a first approximation, this can be obtained by imposing the frequency of the two parallel resonances. The parameter values resulting from the fitting procedure applied to the proposed three-phase winding model are reported in Table III.

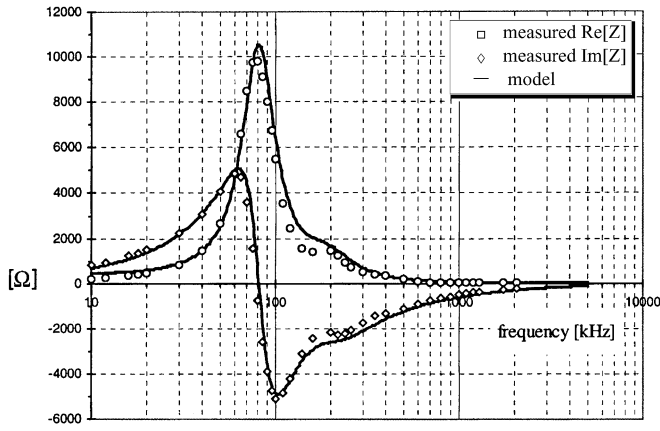


Fig. 4. Real and imaginary parts of the phase-to-phase impedance.

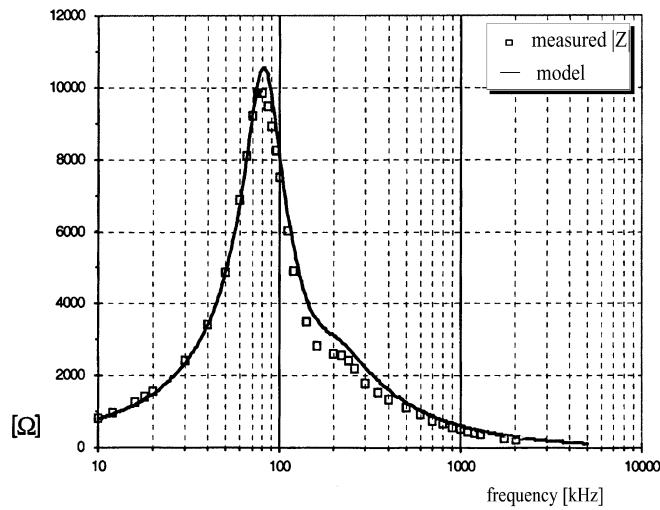


Fig. 5. Magnitude of the phase-to-phase impedance.

C. Impedance Measurements

To verify the proposed model for three-phase motor windings, impedance measurements were carried out at the induction motor terminals with the inverter disconnected. The motor data are given in Table II. The frequency behavior of both phase-to-phase and phase-to-ground impedances was investigated. The measurements were performed by a RLC meter HP 4192 with the frequency ranging from ten kHz to few MHz. The calculated and measured impedance values are shown in Figs. 4–7. Figs. 4 and 5 are related to the phase-to-phase impedance. Figs. 6 and 7 illustrate the behavior of the phase-to-ground impedance. The solid lines represent the numerical results obtained with the circuit model, fitted on the basis of the initial parameter estimation described above, whereas the markers indicate the measured values.

It can be noted that the agreement between numerical and experimental results is good in a wide frequency range even if all the circuit parameters are assumed to be independent of frequency. In order to improve the model matching for frequencies of few tens of kilohertz, frequency-dependent parameters should be adopted. In particular, a better fitting could be obtained by modeling skin and proximity effects in the winding with frequency-dependent resistances, and introducing

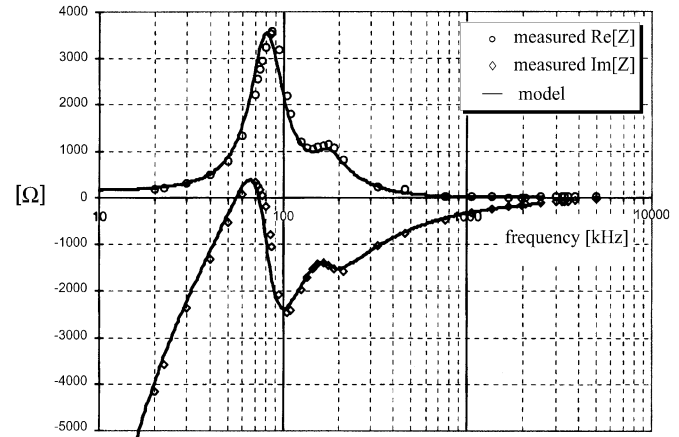


Fig. 6. Real and imaginary parts of the phase-to-ground impedance.

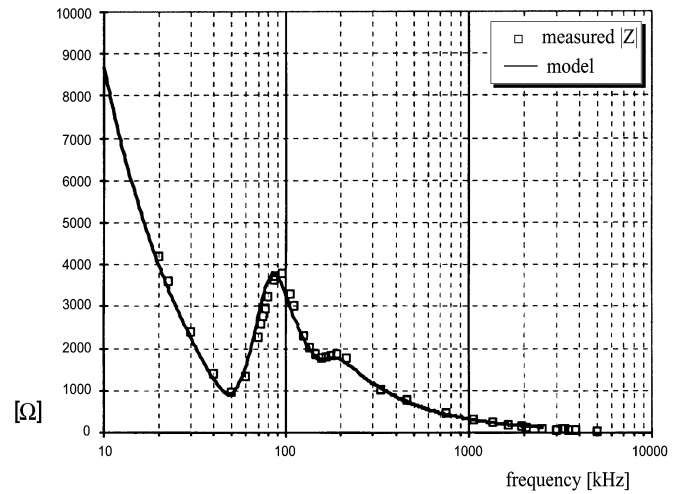


Fig. 7. Magnitude of the phase-to-ground impedance.

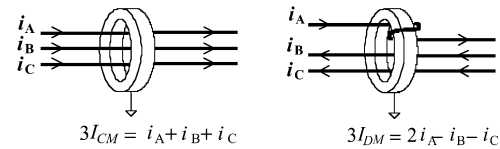


Fig. 8. Arrangement for the CM and DM current measurement for the three-wire system (ac side).

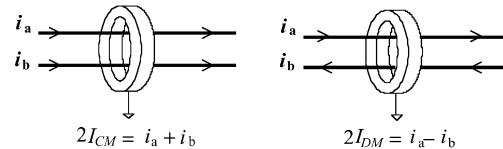


Fig. 9. Arrangement for the CM and DM current measurement for the two-wire system (dc side).

frequency-dependent inductances to account for the magnetic reaction of eddy currents in the laminated iron core. The circuit model with frequency-dependent parameters could be usefully employed for frequency-domain analysis, whereas its application for time-domain analysis could be laborious. It was verified that in most cases the improvements of the results obtained do not justify the increased model complexity.

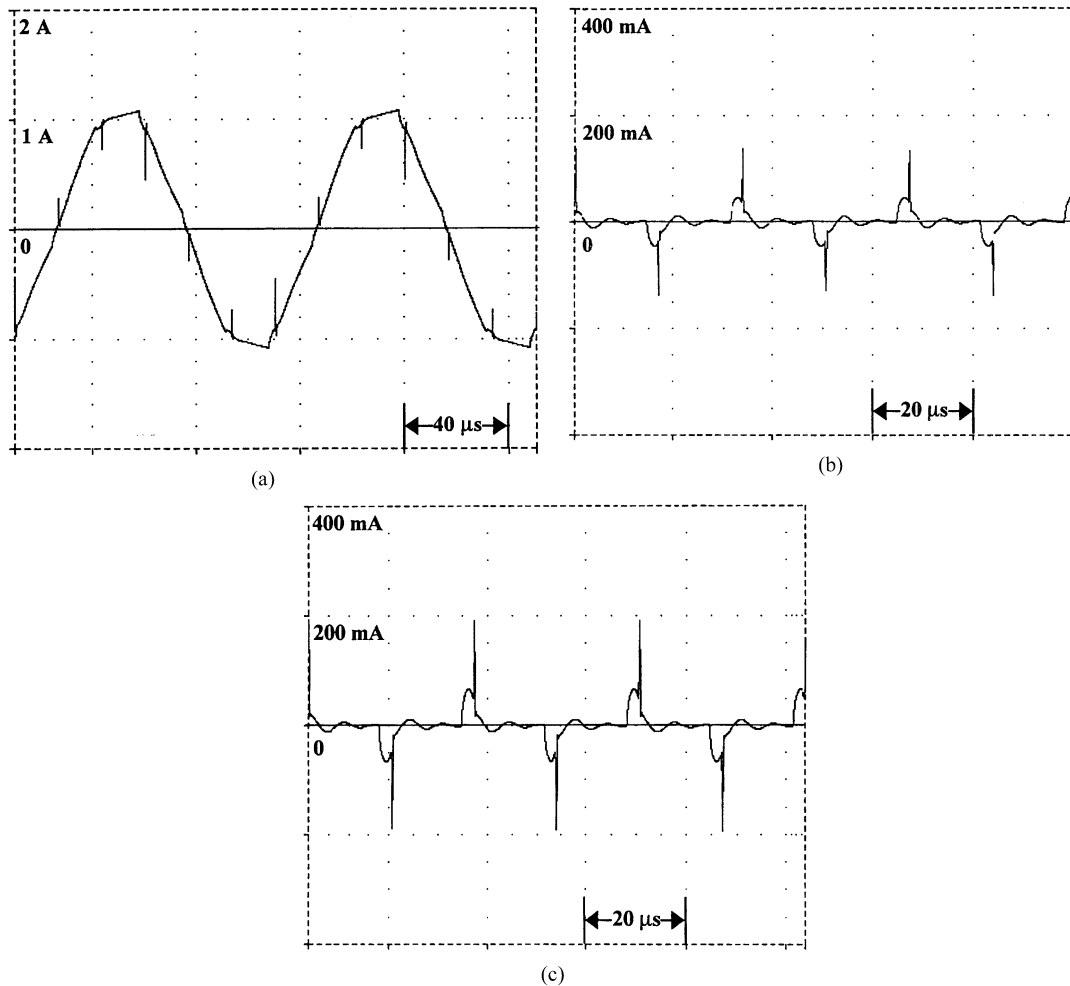


Fig. 10. Numerical results: (a) $3I_{DM}$ at ac side, (b) $3I_{CM}$ at ac side, and (c) $2I_{CM}$ at dc side.

III. CM AND DM CURRENT DETECTION

The conducted interferences are analyzed both at the dc side, between the LISNs and the inverter, and at the ac side, between the inverter and the motor terminals.

For the two-wire system (dc side in Fig. 1), the CM and DM current components are defined by the current signals i_a and i_b as

$$I_{CM} = \frac{1}{2}(i_a + i_b); I_{DM} = \frac{1}{2}(i_a - i_b). \quad (1)$$

For the three-wire system (ac side in Fig. 1), the CM current component is defined by the phase current signals i_A , i_B , and i_C as

$$I_{CM} = \frac{1}{3}(i_A + i_B + i_C). \quad (2)$$

The DM current components can be defined for each phase as

$$I_{DM_k} = i_k - I_{CM}, \quad \text{for } k = A, B, C. \quad (3)$$

For phase A the previous equation yields

$$I_{DM_A} = I_{DM} = \frac{1}{3}(2i_A - i_B - i_C). \quad (4)$$

Equation (4) is used to define the three-phase DM current component for balanced operating conditions.

The conducted interferences are measured by HF current probes. When using magnetic probes with toroidal shape, a proper wire arrangement can be utilized to measure the CM and DM current components. Figs. 8 and 9 show the wire arrangements for three-wire and two-wire systems, respectively. In this way, a multiple of the CM and DM currents is directly measured avoiding an additional analog circuitry that could limit the bandwidth of the measuring system.

IV. NUMERICAL AND EXPERIMENTAL RESULTS

To validate the HF circuit model for the whole system, a prototype of inverter-fed ac motor drive was realized. Measurements in both time and frequency domain were carried out. The inverter was controlled in the “six-step mode” with a fundamental frequency of 10 kHz, that is the lower limit for the validity of the proposed HF circuit model. In this way, only current harmonics with frequency higher than 10 kHz flow in the system under investigation.

The LISNs ($50 \Omega/50 \mu\text{H}$) have been introduced in order to decouple and standardize the inverter input from the dc source. The results presented in this paper were obtained using a battery as dc source. The adopted measuring system was a Tektronix

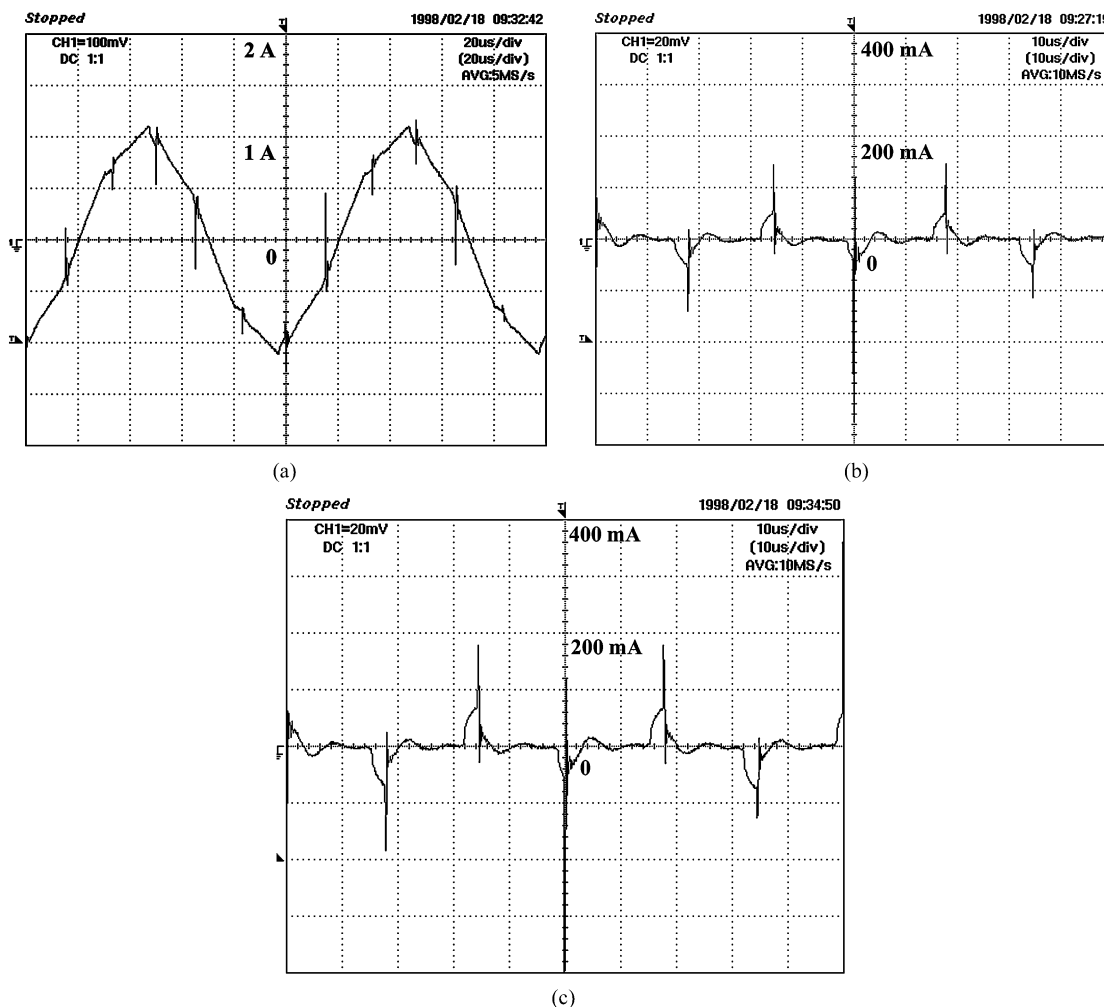


Fig. 11. Experimental results: (a) $3I_{DM}$ at ac side, (b) $3I_{CM}$ at ac side, and (c) $2I_{CM}$ at dc side.

A6303 current probe (bandwidth from dc to 15 MHz) with the corresponding Tektronix AM 503B current probe amplifier. The measuring points are represented in Fig. 1 and the wire arrangements are shown in Figs. 8 and 9.

A. Time-Domain Analysis

The time-domain simulations were carried out by PSpice with an integration step ceiling of 50 ns. The corresponding experimental results have been recorded by a digital oscilloscope with a 50Ω input impedance adapter. The results are shown in Figs.10 and 11, respectively. The agreement is good even if the dependence of all the model parameters on the excitation frequency is neglected. This assumption allows numerical results to be achieved by a standard circuit simulator within reasonable computational times.

Figs.10(a) and 11(a) represent the DM current at the ac motor side. The current waveform is piecewise-linear and the frequency of its fundamental component is 10 kHz. The spikes are due to capacitive currents flowing through the phase-to-phase capacitive coupling owing to the high voltage time derivative (dv/dt) during the IGBTs commutations. It can be noted that the agreement is good for the amplitude of the fundamental component (1 A, 10 kHz), whereas the linear segments have lightly different slopes. The explanation can

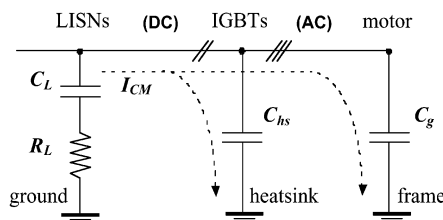


Fig. 12. Common-mode current paths.

be found in Section II-C with reference to Figs. 4 and 5: at 10 kHz the motor model has a good matching as regards the measured magnitude of the phase-to-phase impedance (Fig.5), but the agreement is not so good for its real and imaginary parts (Fig.4).

Figs. 10(b) and 11(b) represent the CM current at the ac side. The waveform periodicity corresponds to a fundamental frequency of 30 kHz. Also in this case, the high dv/dt during the IGBTs commutations is responsible for the current spikes. The current oscillation following each spike has a frequency of about 100 kHz. This value corresponds to the resonant frequency of the phase-to-ground impedance shown in Figs. 6 and 7. The agreement between the numerical and the experimental results is very good.

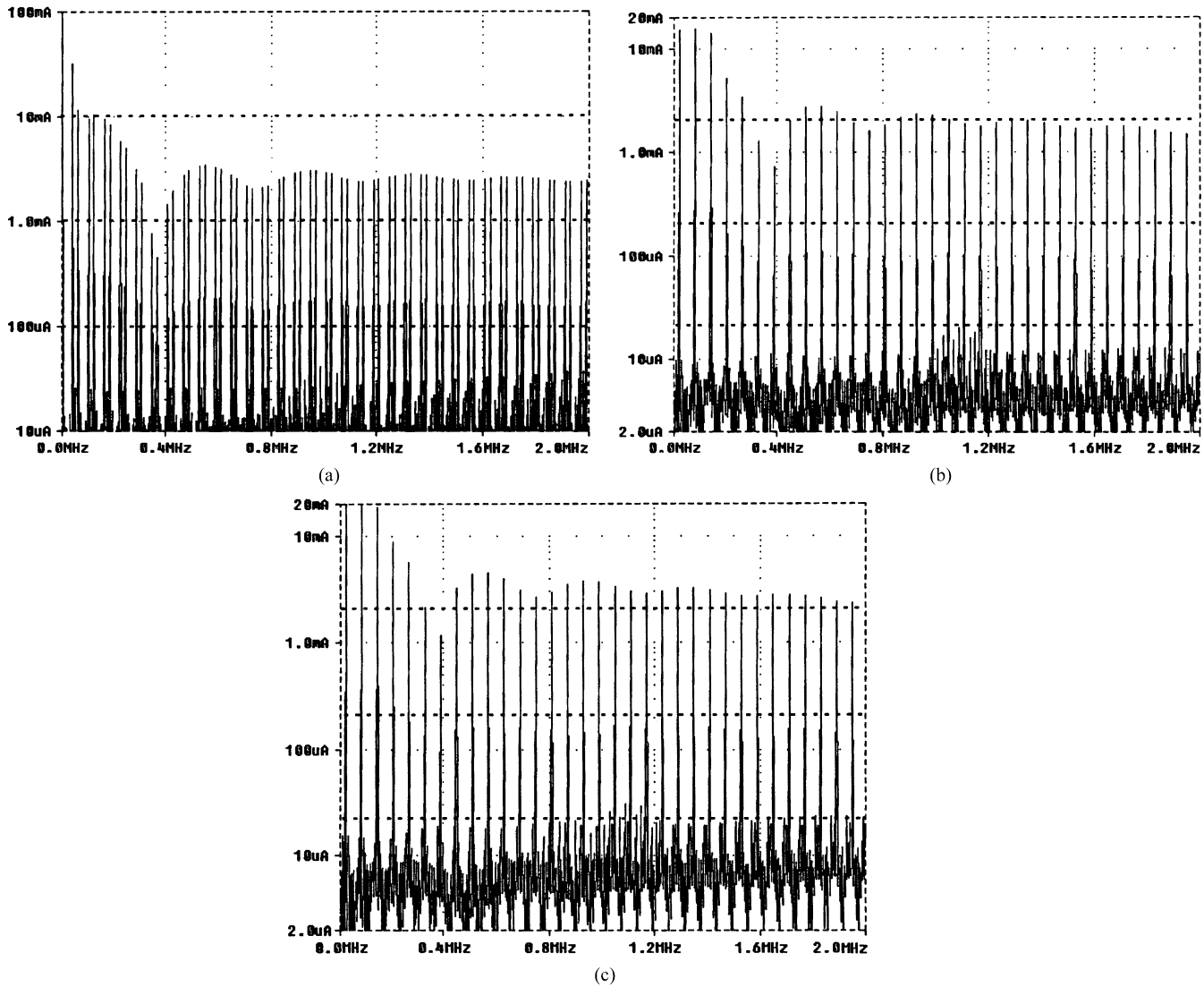


Fig. 13. Numerical results: (a) $3I_{DM}$ at ac side, (b) $3I_{CM}$ at ac side, and (c) $2I_{CM}$ at dc side.

Figs. 10(c) and 11(c) represent the CM current at the dc side. It can be noted that these waveforms practically coincide with the CM current waveforms at the ac motor side except for a small scale factor. This increase at the dc side is due to an additional CM current flowing through the IGBTs-to-heatsink parasitic capacitances (the heatsink is grounded for safety). The CM current paths are shown in Fig. 12. Also in this case the circuit model is able to predict the HF currents with a good accuracy.

The DM current at the dc side is not shown since its amplitude is two order of magnitude less than that of the CM current in the considered range of frequency. This is due to the filtering action performed by the dc capacitors (Table I and Fig. 2) that confine the DM currents inside the loops consisting of the switching legs and the capacitor branches.

B. Frequency-Domain Analysis

The numerical analysis in the frequency domain was performed by post-processing the data obtained in the corresponding time-domain analysis. In this case, the Fourier facility of PSpice was usefully employed. The experimental results were obtained by a HP 8591E spectrum analyzer (bandwidth from 9 kHz to 1.8 GHz).

The measurement were carried out selecting the “peak mode.” The frequency range was 10kHz–2MHz and the results are shown in Figs. 13 and 14.

The fundamental frequency of the DM current components is 10 kHz. In particular, the numerical results represented in Fig.13(a) show that the order of the harmonics is $6k \pm 1$ with k an integer (i.e., 50 and 70 kHz, 110 and 130 kHz etc.). The agreement with the corresponding experimental results represented in Fig. 14(a) is good. It can be noted that the amplitude envelope of the DM current harmonics is very similar in the two cases, but additional harmonic components can be recognized in the experimental results.

The CM current components have a fundamental frequency of 30 kHz. Fig. 13(b) and (c) shows that the harmonic order is $2k + 1$ with k an integer (i.e., 90, 150, and 210 kHz, etc.). The agreement with the corresponding experimental results represented in Fig. 14(b) and (c) is good. Also in this case, the calculated and measured amplitude envelopes of the CM current harmonics are very similar. Additional harmonic components appear in the experimental results. It can be noted that the harmonic amplitudes are increased of about 3 dB at the dc side

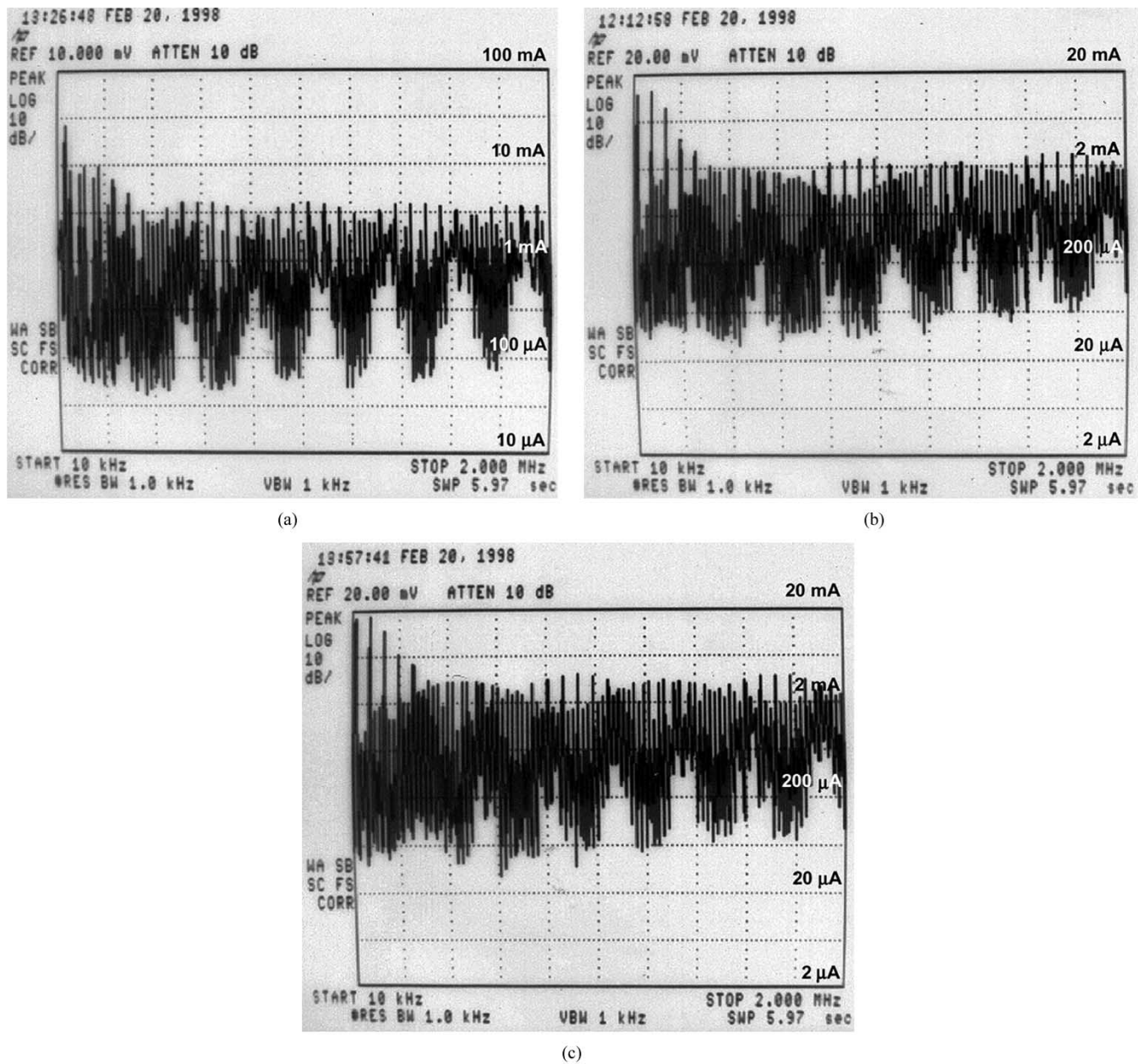


Fig. 14. Experimental results: (a) $3I_{DM}$ at ac side, (b) $3I_{CM}$ at ac side, and (c) $2I_{CM}$ at dc side.

with respect to the ac side owing to capacitive currents through the grounded heatsink, as it could be expected by the scheme of Fig.12.

V. CONCLUSION

In this paper, an inverter-fed ac motor drive has been analyzed with reference to the conducted electromagnetic interferences at both the dc and ac sides of the inverter. Two LISNs have been employed to decouple the dc source from the inverter. HF lumped equivalent circuits for the inverter and the motor stator windings have been proposed. The inverter model includes parasitic elements of power switches, passive components and connecting wires. The circuit model of the motor windings takes account of turn-to-turn and turn-to-ground stray capacitances. The motor model fitting is based on phase-to-phase and phase-to-

ground impedance measurements. The overall system model has been tested by an inverter-fed ac motor drive, considering a 10 kHz six-step modulated inverter.

As the parameter values of the overall system model are obtained from proper measurements, analytical formulas and well-known fitting procedures, the proposed model can be applied to many types of inverters and ac motors, even if the practical results are presented for a specific case.

Using the equivalent circuit presented in this paper, the time-domain analysis can be performed with standard circuit simulators. The proposed model is particularly useful for predicting differential- and common-mode components of conducted EMI in a wide frequency range (10 kHz–2 MHz). Guidelines for an overall system design satisfying the international EMC standards can be derived. In particular, it has been shown that the CM current components strongly affect conducted emissions.

The circuit model allows the effects of EMI suppression filters to be predicted by numerical simulations.

REFERENCES

- [1] L. Gubbala, A. von Jouanne, P. Enjeti, C. Singh, and H. Toliyat, "Voltage distribution in the windings of an AC motor subjected to high dv/dt PWM voltages," in *Proc. PESC Conf.*, Atlanta, GA, June 1995, pp. 579–585.
- [2] Z. Krzemien, "The additional phenomena which appear in induction motors fed from PWM inverters," in *Proc. Eur. Conf. Power Electron. Applicat.*, Trondheim, Norway, Sept. 1997, pp. 2.515–2.519.
- [3] D. Maly, D. W. Novotny, and C. Thompson, "The influence of winding capacitance on high frequency time harmonic losses in induction motors," *Proc. IEEE*, pp. 33–39.
- [4] Y. Murai, T. Kubota, and Y. Kawase, "Leakage current reduction for a high-frequency carrier inverter feeding an induction motor," *IEEE Trans. Ind. Applicat.*, vol. 28, pp. 858–863, July/Aug. 1992.
- [5] E. Zhong, S. Chen, and T. A. Lipo, "Improvements in EMI performance of inverter-fed motor drives," in *Proc. APEC*, Mar. 1994, pp. 608–614.
- [6] E. Zhong, T. A. Lipo, J. R. Jaeschke, and D. Gritter, "Analytical estimation and reduction of conducted EMI emission in high power PWM inverter drives," in *Proc. PESC Conf.*, Baveno, Italy, June 1996, pp. 1169–1175.
- [7] L. Ran, S. Gokani, J. Clare, K. J. Bradley, and C. Christopoulos, "Conducted electromagnetic emissions in induction motor drive systems. Part I: Time domain analysis and identification of dominant modes, Part II: Frequency domain models," *IEEE Trans. Power Electron.*, vol. 13, pp. 757–776, July 1998.
- [8] G. Skibinski, J. Pankau, R. Sladky, and J. Campbell, "Generation, control and regulation of EMI from AC drives," in *Proc. IEEE Ind. Applicat. Conf.*, vol. 2, pp. 1571–1583.
- [9] A. Consoli, G. Oriti, and A. Testa, "Induction motor modeling for common mode and differential mode emission evaluation," in *Proc. IEEE IAS Conf.*, San Diego, CA, Oct. 1996, pp. 595–599.
- [10] S. Ogasawara and H. Hirofumi, "Modeling and damping of high-frequency leakage currents in PWM inverter-fed AC motor drive systems," *IEEE Trans. Ind. Applicat.*, vol. 32, pp. 1105–1114, Sept./Oct. 1996.
- [11] L. Tihanyi, *Electromagnetic Compatibility in Power Electronics*. New York: IEEE Press, 1995.
- [12] G. Grandi, I. Montanari, and U. Reggiani, "Effects of power converter parasitic components on conducted EMI," in *Proc. Int. Zurich Symp. EMC*, Zurich, Switzerland, Feb. 18–20, 1996, pp. 499–504.
- [13] M. T. Wright, S. J. Yang, and K. McLeay, "General theory of fast-fronted interturn voltage distribution in electrical machine windings," *Proc. Inst. Elect. Eng. B*, vol. 130, no. 4, pp. 245–256, July 1983.
- [14] R. G. Rhudy, E. L. Owen, and D. K. Sharma, "Voltage distribution among the coils and turns of a form wound AC rotating machine exposed to impulse voltage," *IEEE Trans. Electron. Compat.*, vol. EC-1, pp. 50–60, June 1986.
- [15] G. Grandi, D. Casadei, and U. Reggiani, "Equivalent circuit of mush wound ac windings for high frequency analysis," in *Proc. ISIE Conf.*, Guimaraes, Portugal, July 1997, pp. SS.201–SS.206.
- [16] G. Grandi, D. Casadei, and A. Massarini, "High frequency lumped parameter model for AC motor windings," in *Proc. Eur. Conf. Power Electron. Applicat.*, Trondheim, Norway, Sept. 1997, pp. 2.578–2.583.
- [17] S. Guttowski, H. Jorgensen, and K. Heumann, "The Possibilities of reducing conducted line emissions by modifying the basic parameters of voltage-fed pulsed inverters," in *Proc. IEEE PESC'97*, St. Louis, MO, June 1997, pp. 1535–1540.
- [18] J. L. Guardado and K. J. Cornik, "Calculation of machine winding electrical parameters at high frequencies for switching transient studies," *IEEE Trans. Energy Conv.*, vol. 11, pp. 33–40, Mar. 1996.
- [19] G. Skibinski, R. Kerkman, D. Leggate, J. Pankau, and D. Schlegel, "Reflected wave modeling techniques for PWM AC motor drives," in *Proc. Appl. Power Electron. Conf. APEC'98*, vol. 2, 1998, pp. 1021–1029.
- [20] G. Suresh, H. A. Toliyat, D. A. Rendusara, and P. N. Enjeti, "Predicting the transient effects of PWM voltage waveform on the stator windings of random wound induction motors," *IEEE Trans. Power Electron.*, vol. 14, pp. 23–30, Jan. 1999.
- [21] *Circuit Analysis Reference Manual, Circuit Analysis Users's Guide with Schematics*, Apr. 1995. MicroSim PSpice.
- [22] T. W. Thorpe, *Computerized Circuit Analysis with Spice*. New York: Wiley, 1992.
- [23] P. A. Chatterton and M. A. Houlden, *EMC: Electromagnetic Theory to Practical Design*. New York: Wiley, 1992.



Gabriele Grandi (M'99) was born in Bologna, Italy, in 1965. He received the M.Sc. (with honors) and Ph.D. degrees in electrical engineering from the Faculty of Engineering, University of Bologna, Italy, in 1990 and 1994, respectively.

In 1995, he joined the Department of Electrical Engineering, University of Bologna, as a Research Associate. Since 2000, he has been a Lecturer of power electronic circuits. His research interests include modeling, simulation, and design of electronic power converters, with particular reference to power conditioning systems for renewable energy resources. Further topics of interest concern EMC problems related to switching converters and circuit models of HF components. He is the author of about 50 papers published in technical journals and conference proceedings.



Domenico Casadei (A'01) received the Laurea degree (with honors) in electrical engineering from the University of Bologna, Italy, in 1974.

He joined the Institute of Electrical Engineering, University of Bologna, in 1975. From 1975 to 1985, he was a Research Assistant, and since 1985, he has been an Associate Professor of electrical drives. He is now full Professor of electrical drives in the Department of Electrical Engineering, University of Bologna. His scientific work is related to electrical machines and drives, linear motors, Maglevs, and power electronics. He has published extensively in technical journals and conference proceedings. Since 1994, he has been a member of the International Editorial Board of the *Electromotion Journal*. His present research interests include direct torque control of induction motors, brushless motors, matrix converters, and power quality.

Dr. Casadei is a member of the IEEE Industrial Electronics and IEEE Power Electronics Societies and the Italian Electrotechnical and Electronic Association (AEI). He is a Registered Professional Engineer in Italy.



Ugo Reggiani (M'92) received the Laurea degree (with honors) in electrical engineering from the University of Bologna, Italy, in 1969.

In 1971, he joined the Faculty of Engineering, University of Bologna, where he was Assistant until 1974 and Assistant Professor until 1980. Since 1980, he has been a Full Professor of electrotechnics with the same Faculty. He was Head of both the Institute of Electrotechnics from 1989 to 1995, and the Department of Electrical Engineering from 1995 to 2001. He was Coordinator of the Doctorate in Electrical Engineering at the University of Bologna from 1988 to 1998. Currently, he is also Adjunct Professor at the University of Modena and Reggio Emilia. His main research interests concern electromagnetic field theory, magnetic system studies, electromagnetic compatibility, electrical machines and drives, circuit analysis and modeling of switched networks.

Dr. Reggiani is a member of the IEEE Power Electronics Society and the Italian Electrotechnical and Electronics Association (AEI).